Research Paper

GEOSPHERE

GEOSPHERE; v. 15, no. 1

https://doi.org/10.1130/GES01574.1

12 figures; 2 tables

CORRESPONDENCE: brian.burnham@abdn.ac.uk

CITATION: Burnham, B.S., and Hodgetts, D., 2018, Quantifying spatial and architectural relationships from fluvial outcrops: Geosphere, v. 15, no. 1, https://doi.org/10.1130/GES01574.1.

Science Editor: Shanaka de Silva
Associate Editor: Lesli Wood

Received 14 June 2017
Revision received 1 June 2018
Accepted 26 October 2018

Quantifying spatial and architectural relationships from fluvial outcrops

Brian S. Burnham*,† and David Hodgetts†

School of Earth and Environmental Sciences, The University of Manchester, Manchester, M13 9PL, UK

ABSTRACT

Outcrop analogue studies allow detailed investigation of sandstone body geometry and architecture within fluvial systems. Characterization of these elements is fundamental to understanding and quantifying sandstone body connectivity within hydrocarbon reservoir models, and hence improving recovery from those reservoirs being modeled. This study utilized a laterally and vertically continuous terrestrial light detection and ranging (lidar) data set from the La Serrata section of the Oligocene–Miocene Huesca fluvial fan, in the Ebro Basin in Spain. This data set was used to create a high-resolution three-dimensional digital outcrop model of a 2 km² cliff section representing the heterogeneity in the medial (midfan) portion of a large fluvial fan. Geostatistical information (i.e., sandstone body width and thickness) extracted from the models using quantitative analytical techniques, integrated with traditional sedimentary log data, allowed the calculation of probability density functions of 42 sandstone bodies from corrected (true) width measurements. These data show that sandstone bodies are up to 6 m thicker and 209 m wider than previous studies have estimated. Furthermore, an observed temporal trend of thickening and widening of sandstone bodies up section before a reduction in the uppermost portion provides evidence for possible avulsion events. These data, compared with previous studies of this and other fluvial systems, illustrate the efficacy of digital outcrop models as quantitative tools for accurate characterization of critical reservoir elements from outcrop analogues.

INTRODUCTION

Fluvial systems have long been recognized as important sedimentary deposits in the rock record because they may contain large reserves of hydrocarbons (Miall, 1988; North and Taylor, 1996; Bridge and Tye, 2000). Recent studies suggest that distributive fluvial systems comprise most of the recognized fluvial geometries of aggradational continental basins (Hartley et al., 2010; Weissmann et al., 2010). Hartley et al. (2010) defined a distributive fluvial system as a fluvial system that (1) displays a radial distributive pattern in planform, (2) often does not contain simultaneously active channels, and (3) encompasses a range of scales of alluvial and fluvial distributive landforms, from alluvial fans to megafans (Weissmann et al., 2015). Recent work has also indicated that detailed quantitative analysis of distributive fluvial system deposits, from basin to regional scale, is required to better understand the spatial distribution of the associated sandstone body geometries (Owen et al., 2015; Hartley et al., 2015). To that end, conventional one-dimensional (1-D) well log and borehole data from fluvial systems make constraining fluvial stratigraphic architecture difficult over basin-wide scales (e.g., Ryseth et al., 1998; Donselaar et al., 2011; Kukulski et al., 2013), and conventional seismic data cannot resolve sandstone body geometries that fall below the minimum resolution (Pranter et al., 2014). Because of this, outcrops are routinely used by geoscientists as analogues to gain insight into stratigraphic fluvial architecture in an effort to quantify spatial heterogeneity (Miall, 1988). The type of outcrop analogue must be chosen carefully however (Alexander, 1993), as they remain problematic due to the inherent three dimensionality of the sandstone body geometry and the limited exposure of the outcrop (Pringle et al., 2004; Pranter et al., 2014). The inherent spatial heterogeneity of sandstone body distribution in outcrop has lead geoscientists to develop methods to quantitatively visualize and analyze outcrops of fluvial successions.

The evolution of integrated geospatial mapping techniques to create digital three-dimensional (3-D) representations of outcrops, or digital outcrop models (DOMs), has seen continued improvement and application to fluvial-related outcrops (e.g., Xu et al., 2000; van Lanen et al., 2009; Fabuel-Perez et al., 2009a; McCaffrey et al., 2010; Rarity et al., 2014). DOMs offer a laterally and vertically continuous high-resolution data set that allows accurate interpretation and interpolation of the data across distances unachievable through traditional approaches (i.e., 1-D sedimentary logs and/or two-dimensional [2-D] photo panels). Moreover, the integration of quantitative mapping and modeling techniques with traditional data has allowed geoscientists to acquire, process, analyze, and visualize high-resolution digital outcrop information better than ever before (e.g., Hodgetts, 2013; Rarity et al., 2014; Rittersbacher et al., 2014). Quantitative outcrop analytical techniques used to analyze the spatial characteristics (i.e., width, thickness, and connectivity) of sandstone bodies within a fluvial succession are critical to the development and/or refinement of conceptual depositional models (e.g., Fabuel-Perez et al., 2009a, 2009b; Durkin et al., 2015) and ultimately accurate analogues used in reservoir modeling practices (e.g., Fabuel-Perez et al., 2010; Labourdette, 2011).

*Current affiliation: School of Geosciences, Department of Geology and Petroleum Geology, The University of Aberdeen, Aberdeen, AB24 3UE, UK
†E-mails: brian.burnham@abdn.ac.uk; david.hodgetts@manchester.ac.uk

In this study, we applied these methods to a section within the 60 km radius of the Oligocene–Miocene Huesca fluvial fan succession in northeast Spain (Fig. 1). This succession offers moderately to well-exposed outcrops of a distributive fluvial system, from proximal to distal sections (Hirst, 1992; Arenas et al., 2001; Fisher and Nichols, 2013). The section used for this study, identified as being within the medial zone of the distributive fluvial system, offers a laterally continuous, nearly 3-D exposure (Fig. 2) of the stratigraphy in a 2 km^2 area (Fig. 3; Hirst, 1992; Fisher and Nichols, 2013), allowing a detailed and quantitative investigation into the sandstone geometry of channel-fill deposits. We undertook a 3-D quantitative spatial analysis of the true width and thickness of individual sandstone bodies through the calculation of probability distribution functions (PDFs) for each measured body and related this to spatial distribution within the section. These spatial statistics may then be used to help model analogous hydrocarbon reservoirs and improve connectivity estimates. A discreet quantitative facies classification scheme by sandstone body type (sensu Gibling, 2006; i.e., multistory, multilateral, and single story) was attributed to the measured sandstone bodies to provide conditioning data when used in facies modeling.

GEOLOGICAL SETTING

The Ebro Basin is a foreland basin of the southern Pyrenees resulting from flexural subsidence of the Iberian crust during uplift in the Cenozoic Pyrenean orogenic belt (Fig. 1; Teixell, 1996). From the early Eocene to early Miocene, the southern Pyrenean zone was an area of southward-trending thrust events, which formed the southern foredeep of the Pyrenees (Nichols, 1987). During the final phase of deformation (late Oligocene), a thrust-sheet frontal ramp developed and created the present-day topographic expression in the External Sierras (Nichols, 1987). This formed the northern margin of the Ebro Basin.

Three mountain ranges surround the Ebro Basin, the Pyrenees to the north, the Catalan Coastal Range to the east, and the Iberian Range to the southwest; it is one of the largest Tertiary basins in the Iberian Peninsula (Fig. 1A; Arenas and Pardo, 1999). In the earliest Oligocene, compressional stress events in the Iberian and Pyrenean ranges cut off the Ebro Basin from drainage into the Bay of Biscay and Atlantic Ocean. The Ebro Basin became an endorheic basin, or an internally draining basin, which remained closed until the late Miocene, allowing a thick accumulation of continental clastic strata within the basin (Hirst and Nichols, 1986).

The three principal source areas for the clastic fill along the northern margin of the Ebro Basin, which make up the coeval Huesca and Luna fluvial fans (Fig. 1B), are the southern Pyrenean zone, the Internal Sierras, and the Pyrenean axial zone (Hirst and Nichols, 1986; Nichols, 1987). Sediments from erosion within the three Pyrenean basins (Jaca, Ainsa, and Tremp-Graus) that occurred during the Oligocene and Miocene mixed with older carbonates from the southern thrust belt and constitute the majority of the Huesca and Luna sequences (Fig. 1A; Hirst and Nichols, 1986; Hirst, 1992). The Huesca and Luna form well-preserved distributive fluvial system successions due to the aggra-

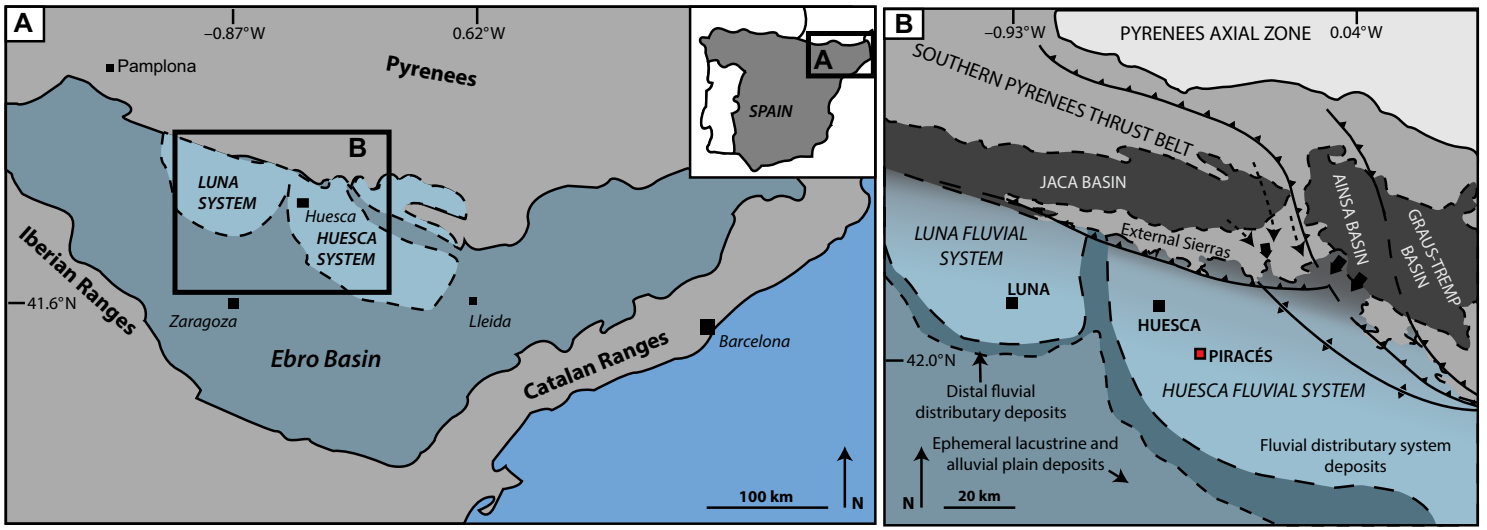

Figure 1. (A) Location map of the study area, showing the Huesca and coeval Luna distributive fluvial systems within the Ebro Basin surrounded by three coastal ranges (Pyrenees, Iberian, and Catalan). (B) The principal source area for the Huesca distributive fluvial system is within the Pyrenees from the Ainsa and Graus-Tremp Basins, while the neighboring Luna system source area is within the Jaca Basin (modified from Hirst and Nichols, 1986; Jones, 2004; Nichols, 2009).

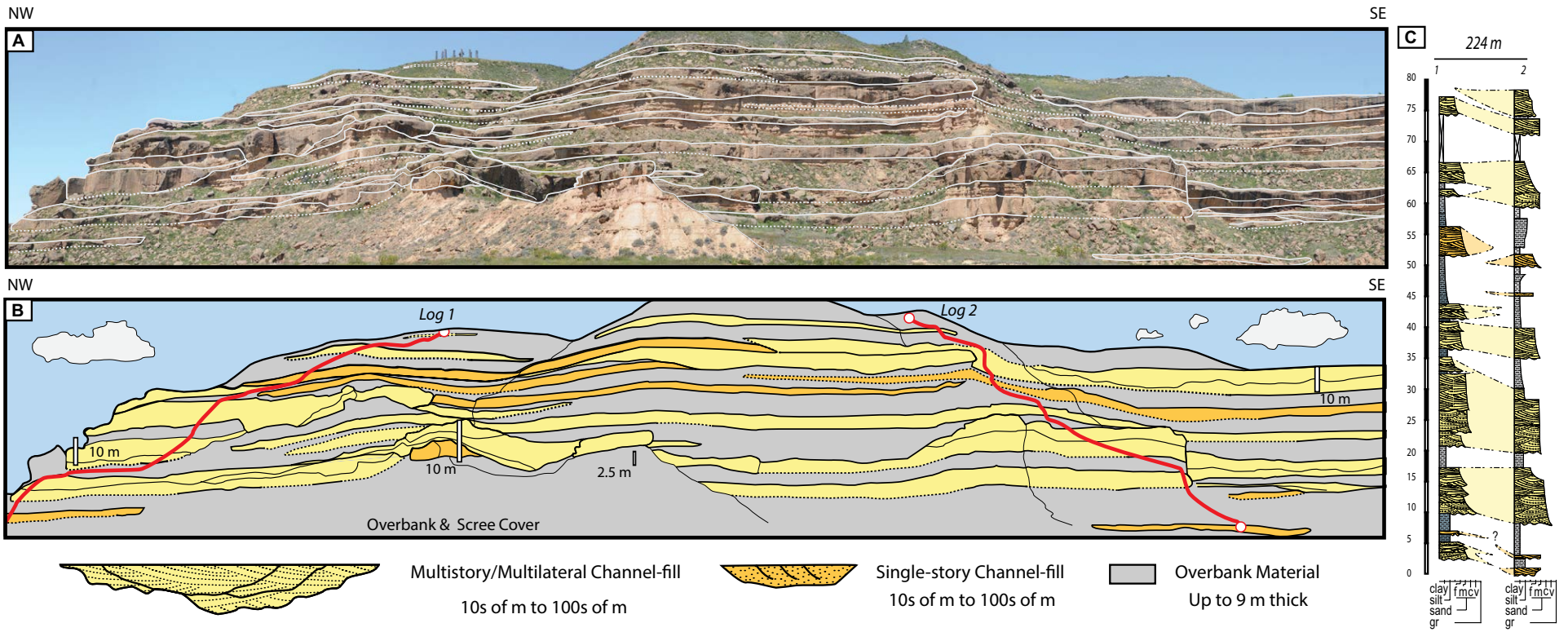

Figure 2. (A) Photo panel illustrating the degree of exposure common in the study area. Lines (light-gray) drawn onto photo panel denote sandstone body outlines. (B) Sketch derived from photo panel in A with colors highlighting the interpreted sandstone body architecture. (C) Two sedimentary logs with log tracts (red lines in B) that highlight the spatial (vertical and lateral) heterogeneity within the section. Abbreviations: gr—gravel; f—fine; m—medium; c—coarse; v—very coarse.

dational nature of the two systems within the endorheic Ebro Basin. The basin remained closed for ~25 m.y. and would not reopen to drain into the Mediterranean Sea until the late Miocene (Garcia-Castellanos et al., 2003).

Sedimentation of the Huesca Fluvial Fan

The Huesca fluvial fan developed through a process of continual avulsion of river systems into depositional lobes across the floodplain, creating a large (60 km) fan morphology in plan view (Fig. 4; Hirst, 1992; Nichols and Fisher, 2007; Weissmann et al., 2015; Fisher and Nichols, 2013). The Huesca system is identified as having a low-gradient longitudinal profile that is controlled by an ephemeral lake in the center of the basin, which behaved as the ultimate base-level control (Nichols and Hirst, 1998; Nichols, 2004; Arenas et al., 2001). This low gradient promotes continued avulsion of the active river tracts across the alluvial plain, resulting in progressive sediment accumulation and aggradation into the basin. As sediment accumulates in the basin, sedimentary loading may cause regional subsidence, but if the sediment supply exceeds the rate of subsidence, the system will aggrade, and subsequent base level will rise (Nichols, 2004, 2007; Fisher and Nichols, 2013), which has been identified in the Ebro Basin. Moreover, the lack of evidence for lateral confinement of channel belts or incised valley patterns in the Huesca system deposits (Hirst, 1992) indicates deep fluvial incision into the strata did not occur, suggesting minimal change in the consistent aggradation of the base level. Without an external connection to a sea, sediment was allowed to accumulate until the basin spill point was reached (Nichols, 2004).

The Huesca fluvial fan is characterized by three zones: proximal, medial, and distal, which are defined by the change in gross stratigraphic architecture across the system (Fig. 4A; Hirst and Nichols, 1986; Nichols, 1987). Erosion following uplift of the Barbastro anticline removed the proximal deposits of the Huesca fan, but inferences of clast size and channel dimensions can be made

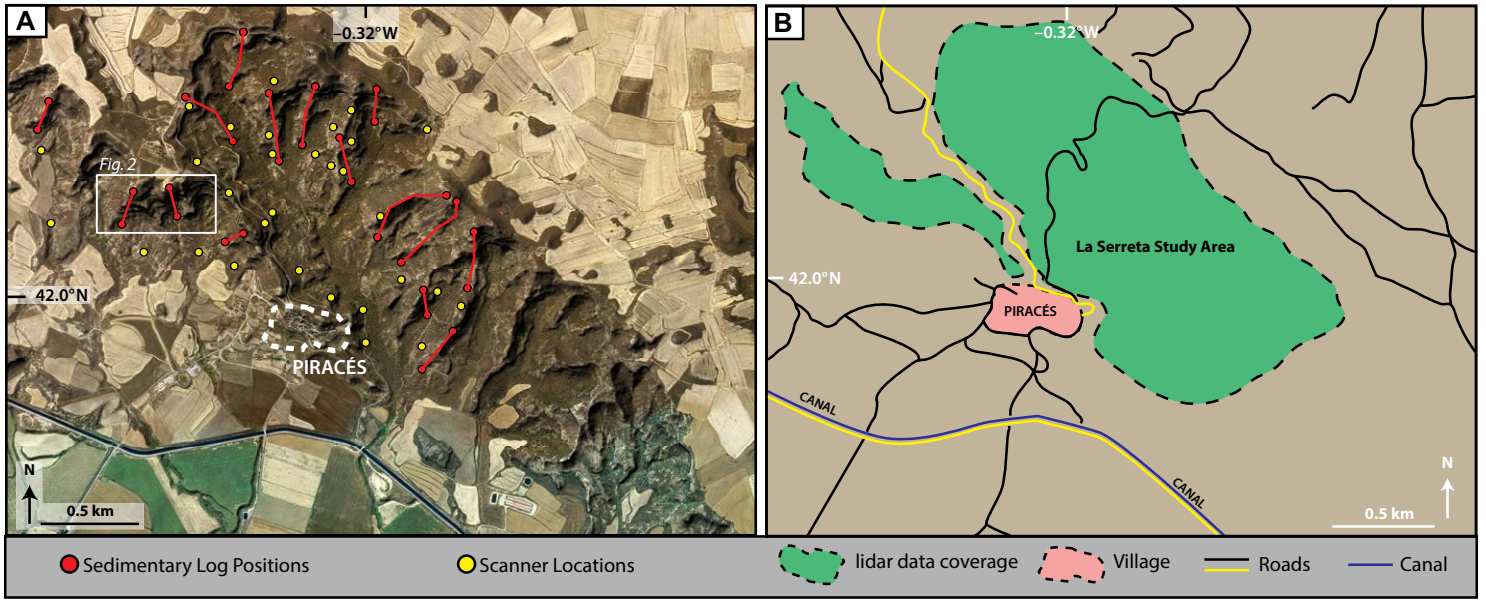

Figure 3. (A) Orthophotograph of the La Serreta study area with approximate light detection and ranging (lidar) scan locations (yellow) and sedimentary log positions and associated tracts (red; Centro Nacional de Información Geográfica [CNIG] [C.I.F.: Q-2817024-I C—General Ibáñez de Ibero, 3. 28003, Madrid, Spain, https://www.cnig.es/]; orthoimagery was accessed 15 April 2013; base map retrieved 17 April 2013; this particular imagery was published 2 October 2012). (B) Schematic of La Serreta area highlighting approximate lidar data coverage area.

by examining deposits from the similar and coeval Luna fan (Nichols, 1987). The medial zone is composed of relatively homogeneous, very coarse- to medium-grain-size sandstone in channel-fill deposits, surrounded by overbank siltstone and mudstone with thin sheets of fine to very fine sandstone (Fig. 4B). The sandstone bodies identified in this zone are up to 10 m thick, with an average thickness of 3 m (Hirst, 1992). These deposits are interpreted as remnants of multistory scour-and-fill ribbon channels that meandered across the floodplain (Nichols and Fisher, 2007). In the distal zone of the Huesca system, the proportion of channel-fill elements to overbank deposits is much lower and is dominated by thin sheets of fine-grained sandstone bodies surrounded by siltstone and mudstone deposits. Identified channel-fill elements have a maximum thickness of 3.5 m, averaging 2.18 m. These are interpreted as deposits of terminal splays originating from unconfined flow events onto the dry floodplain (Fisher et al., 2007).

Study Area

The La Serreta study area is located near the city of Piracés in northeast Spain, where there is a continuous amphitheater-style exposure (Fig. 3A) over 2 km^2, exposing over 100 m of stratigraphy (see Fig. 2). This area is located within the medial zone of the Huesca system (Fig. 1B), containing channel-fill sandstone bodies that are laterally continuous for hundreds of meters (Fig. 2). The deposits are interpreted as sheetlike or ribbon-shaped channel-fill elements, which consist of very coarse- to fine-grained material (Hirst, 1992; Nichols and Fisher, 2007). Some contain decimeter-scale internal structures, while others show very few or no structures within a single story. A general thickening and coarsening trend up section was observed in other studies, suggesting evidence for progradation of the fluvial fan when it was active in this part of the basin (Donselaar and Schmidt, 2005). Evidence of braid bars was also identified in some of the sandstone bodies, interpreted as midchannel or lateral bars (Donselaar and Schmidt, 2005). The bases of the majority of the channel-fill sandstones, however, are not deeply incised into the floodplain, providing evidence for the lateral mobility of the streams throughout deposition (Hirst, 1992; Sadler and Kelly, 1993).

METHODS

Data Acquisition

A Riegl LMS-Z420i terrestrial laser scanner (TLS) was used to acquire high-resolution point clouds from 30 scan positions (Fig. 3A) to maximize coverage and minimize shadows, or gaps, within the final data set (Fig. 3B).

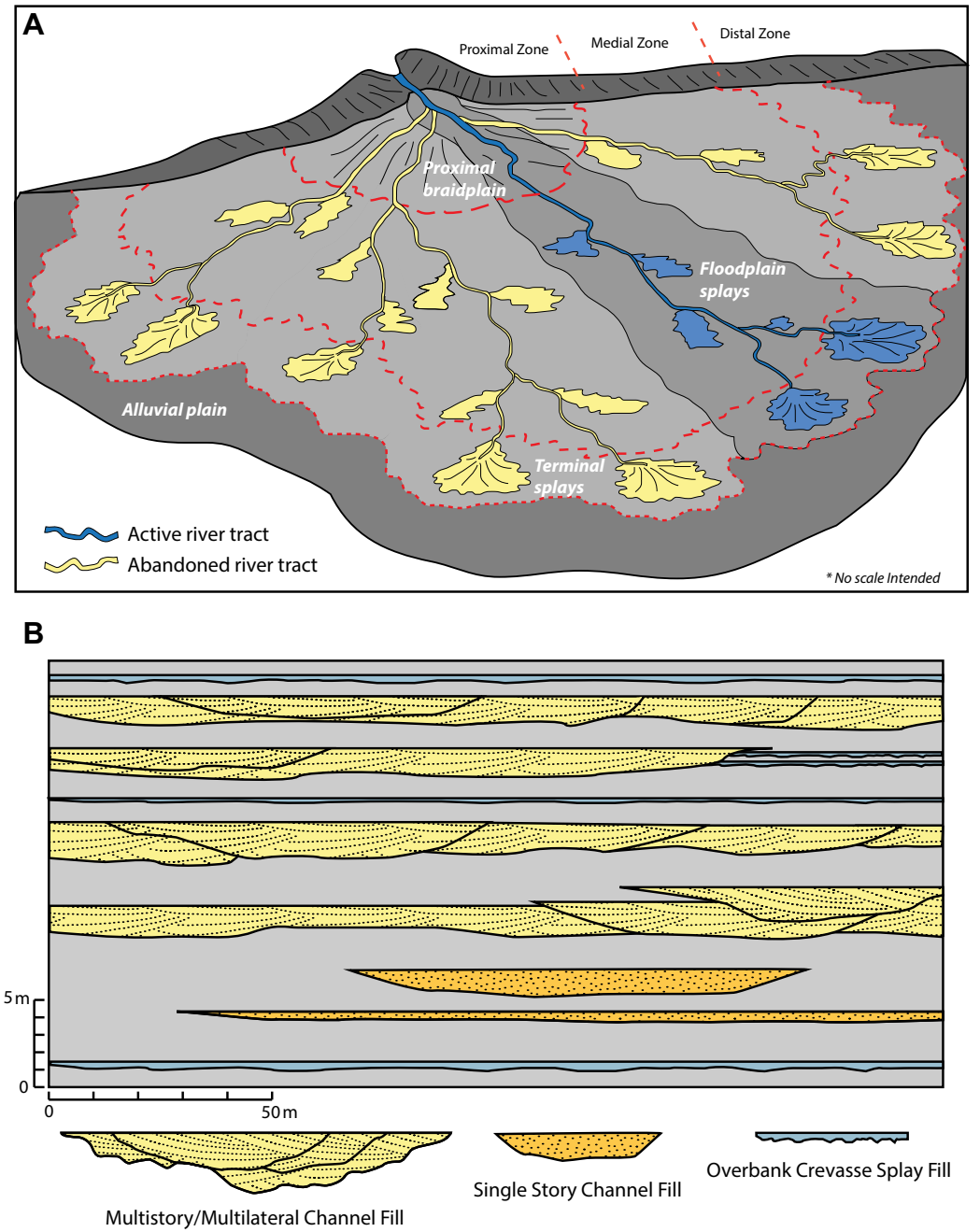

Figure 4. (A) Distributive fluvial system model for Huesca fluvial fan. Note the decrease in channel size and distributary pattern down the fan across the active depositional lobe and subsequent active river tract (modified from Nichols and Fisher, 2007). (B) Sketch of interpreted stratigraphic architecture of the study area (adapted from Nichols and Fisher, 2007). This illustrates several amalgamated and multistory sandstone bodies (yellow), with single-story (orange) geometries as the subordinate type identified. Sandstone bodies are bound by thick accumulations of overbank deposits, which contain crevasse splay elements (blue-gray) composed of very fine-grained sandstone or coarse-grained siltstone.

The high-resolution scans contained a data point spacing of ≥0.10 m, equivalent to ≥0.20 m geometric resolution. A range of lens focal lengths was used for the coaxial camera (e.g., 14 mm, 50 mm, and 85 mm), which made it possible to achieve a pixel-to-pixel match of the red-green-blue (RGB) information to the point cloud.

Fifteen sedimentary logs totaling 800 m of stratigraphy were acquired to help characterize lithological trends across the outcrop (Fig. 2C). These data provided further constraints on facies distribution when constructing the 3-D geologic models. The sedimentary log locations and vertical resolution (0.10 m) were chosen to best represent and test the lateral continuity of the sandstone bodies. In total, 253 paleocurrent measurements were recorded from sedimentary structures (i.e., lateral accretion surfaces, tabular cross-beds, current and climbing ripples).

Differential geospatial navigational satellite system (DGNSS) data points acquired at each TLS location, as well as the top and bottom of each sedimentary log, allowed direct integration of the entire data set into a real-world coordinate frame (at a spatial resolution of 0.60 m; Fig. 3A). This process ultimately resulted in the final realized geologic model spatial constraint for the sandstone body analysis.

Data Processing

Several authors (e.g., Bellian et al., 2005; Enge et al., 2007; Pringle et al., 2006; Buckley et al., 2008; Hodgetts, 2010) have discussed well-established TLS methods and techniques for acquiring, processing, and building accurate DOMs. The processing steps used for this study were:

(1) align the point clouds to real-world coordinates;
(2) colorize the point clouds from the coaxially mounted RGB images;
(3) create a direct triangulation, or triangulated irregular network (TIN), of the data points to create a surface mesh; and
(4) import the data into the geological interpretation software Virtual Reality Geological Studio (VRGS; Hodgetts et al., 2015).

The light detection and ranging (lidar) scans along with the associated TLS DGNSS positions were imported into the software package Innovmetric Polyworks™, version 11, for alignment and georeferencing. The point clouds were colored from the coaxially mounted RGB information using Riegl RiSCAN Pro™ (Fig. 5A). Triangulation of point cloud data into mesh data was completed in VRGS (Fig. 5B).

Visualization

Various methods are available that allow accurate and detailed interpretation and interpolation of the geologic data. Photorealistic models and other visualization methods available in VRGS were used to accurately identify the key features required to quantitatively map and extract sandstone body geometry and statistics. The major advantage of photorealistic DOMs is providing a user with a realization of the model, as one would see it in the field, which allows for a detailed inspection of the color differences in lithology (Figs. 5A and 5B). This color difference plays a significant role because the different lithologies display characteristics that aid in the distinction between overbank (light-brown to light tan) and channel deposits (dark-brown to brown), which can have similar topography but different colors.

Tensor analysis was used to calculate attributes such as coplanarity (Fig. 5C) and dip (Fig. 5D) of the features within the model (e.g., Fernández, 2005; García-Sellés et al., 2011; Rarity et al., 2014; Seers and Hodgetts, 2014). These surface attributes improve the ability of the user to recognize the boundaries of the continuous sandstone body geometries (i.e., coplanarity) and the lateral variability within the models. Surface attributes allow the user to delineate exposed surface boundaries of in situ deposits (e.g., dip = 90°) from vegetation or scree slopes (e.g., dip = 35°) accurately, thus increasing the accuracy of the geostatistics derived from the 3-D models (Fig. 5D). Using surface attributes can also allow recognition and measurement of large sedimentary structures (i.e., bounding surfaces or lateral accretion surfaces) within the sandstone bodies that may not be apparent within a gray-scale model or even a photorealistic model. This technique negates the need for an independent light source that would otherwise require positioning in several orientations to illuminate features that are readily visible in the tensor-analyzed data.

Sandstone Body Mapping and Characterization

The "Geobody" mapping tool in VRGS allows the user to digitize the visible vertical and lateral extents of sandstone bodies throughout the area to investigate their positions in 3-D space, which gives each sandstone body a quantitative spatial context integral for accurate architectural analysis (Burnham and Hodgetts, 2015). Once the sandstone body is bound by a Geobody polygon, field-based sedimentary information such as paleocurrent measurements and other associated sedimentary structures can be attributed to each polygon. The attributed paleocurrent data are used to correct the observed width to the true width by following an approach similar to that of Fabuel-Perez et al. (2009a). This method has been applied in other studies (e.g., Rarity et al., 2014; Rittersbacher et al., 2014), but it was improved herein to produce a more robust statistical data set. Because each geobody is associated with multiple paleocurrent measurements, there is an uncertainty in the direction to be used to calculate the mean paleoflow; therefore, all directions were used to derive a PDF for the corrected width data (Fig. 6). This PDF provides a minimum, maximum, and arithmetic mean (most likely) size for each geobody (Fig. 7). Finally, detailed investigation of the sandstone bodies in both the DOM and sedimentary log data facilitated the classification, based on the scheme provided by Gibling (2006), of the sandstone bodies as either single-story or multilateral and multistory sandstone bodies. A facies code was assigned to the polygons attributed to each sandstone body type (van Lanen et al., 2009).

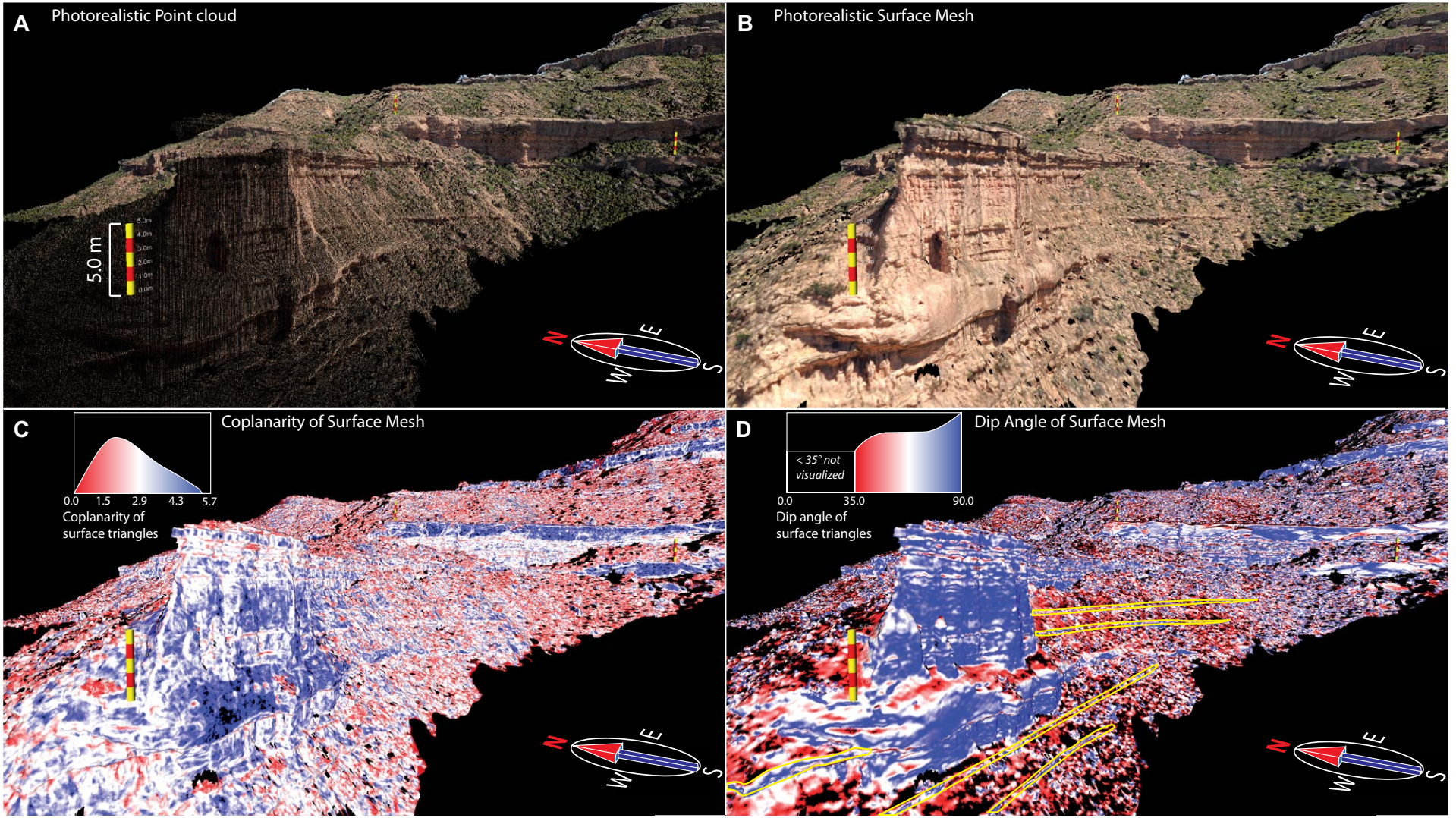

Figure 5. Attribute generation for a portion of the light detection and ranging (lidar) digital outcrop model (DOM) data set, illustrating the variation in lithology and characteristics that can be drawn from the various realizations. Scale bars are 5.0 m in all figures. (A) Red-green-blue (RGB)–colored point cloud from the lidar data set. (B) RGB-colored triangulated mesh derived from the point cloud data set, which visibly preserves the morphology of the DOM, as seen between parts A and B. (C) Coplanarity attribute realization derived from a tensor analysis performed on the DOM mesh to highlight surfaces that have similar planar features. (D) Dip from a triangle orientation derived from a mesh of the DOM. Some crevasse splay features are highlighted (yellow).

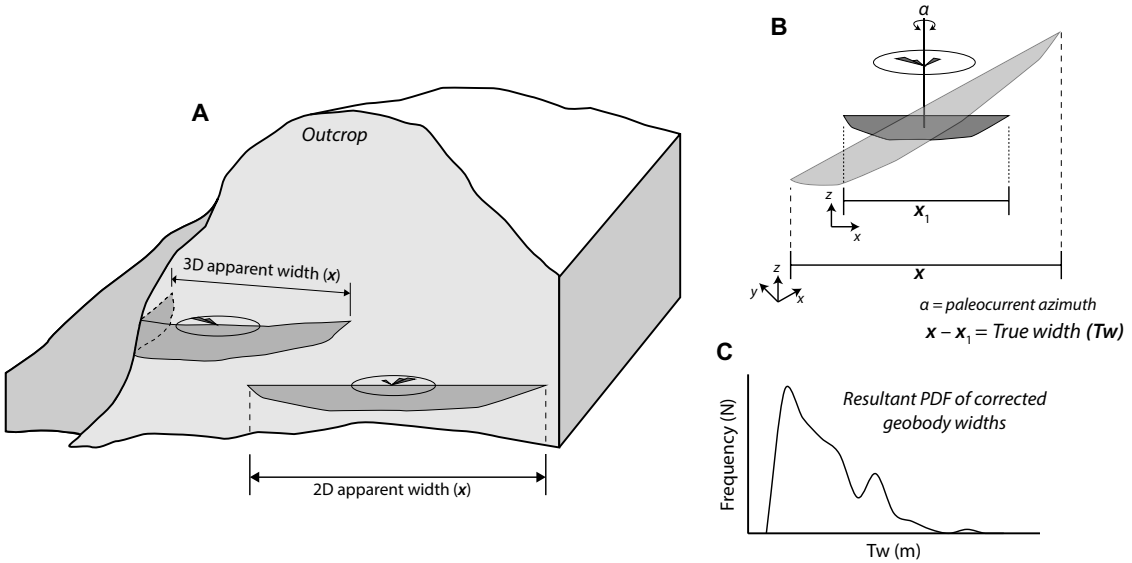

Figure 6. Diagram illustrating the procedure to correct apparent sandstone body width to true width from outcrop-derived sandstone body measurements. (A) Each sandstone body is bound by a geobody polygon, which is used to derive the apparent width, whether it is two dimensional (e.g., single cliff section) or three dimensional (e.g., exposed around a corner of cliff sections). (B) Each digitized geobody is rotated around its *z*-axis until the geobody is orthogonal to a paleocurrent azimuth. The difference calculated between the outcrop-derived apparent (*x*) and rotated geobody (x_1) widths is the true width. Because each geobody is associated with multiple paleocurrent measurements, all associated azimuths are used to derive a probability distribution function (PDF) for the corrected width data. (C) Example of a generated probability distribution function (PDF).

Once assigned, the points within the boundary of the polygon were assigned a discreet value (e.g., point color; Fig. 8). These data provided easy facies recognition when visualized across the data set, as well as essential conditioning data in construction of geocellular and reservoir simulations from the digital outcrop data (Burnham and Hodgetts, 2015).

RESULTS

Histograms (Fig. 7), scatter plots, and curves (Figs. 9–12) were plotted for the sandstone bodies and their spatial position within the La Serreta stratigraphy. These metrics included: (1) calculated sandstone body width PDFs (i.e., minimum, maximum, and arithmetic mean of each sandstone body with a PDF generated for those PDFs) and stratigraphic (i.e., vertical) position, and (2) sandstone body width versus thickness. In order to place the individual geobodies in chronological order, the vertical position of each sandstone body in the overall stacking pattern was determined by examination of the position of that sandstone body in comparison to the sandstone bodies around it. These local observations used in conjunction with the DOM were used to define the chronological order of the sandstone body deposition.

Geobody Width Analysis

The minimum sandstone body width PDF averaged 98 m, with a maximum of 344 m and a standard deviation of 84.2; 76.2% of these sandstone bodies were ≤150 m, with only 19.1% of them distributed between 150 and 300 m (Fig. 7B). The maximum sandstone width PDF averaged 158 m, with a maximum of 525 m and a standard deviation of 125 (Fig. 7C); 59.5% of these sandstone bodies were ≤150 m, while 28.6% were between 150 and 300 m wide. The calculated mean sandstone body width PDF averaged 127 m, with a maximum of 372 m and a standard deviation of 98.6; 69.1% of these sandstone bodies were ≤150 m wide, with 23.8% identified between 150 and 300 m (Fig. 7D). Table 1 provides a summary of the generated statistics.

Plotting the stratigraphic (i.e., vertical) position of each measured sandstone body revealed a vertical trend in sandstone body widths. The sandstone bodies generally increase in width vertically in the middle half of the section (i.e., minimum, maximum, and mean) before decreasing in width near the top one fourth of the section (Fig. 9).

Geobody Width versus Thickness

Observed sandstone body thicknesses were up to 16 m, with a mean of 8 m. Previous works identified the maximum sandstone body thickness measured to be 10 m (Hirst, 1992). However, 11 (26%) sandstone bodies were found to be thicker than the maximum observed by Hirst (1992). Sandstone body width versus thickness values exhibited a positive correlation, with a mean sandstone body width versus thickness (W:T) ratio of 16.1:1, although this correlation is weak (R^2 = 0.5027) given the variability in width distributions (Fig. 10). A periodic sandstone body thickening and thinning up-section trend was observed within an overall general upward thickening and widening trend in the full section (Fig. 11).

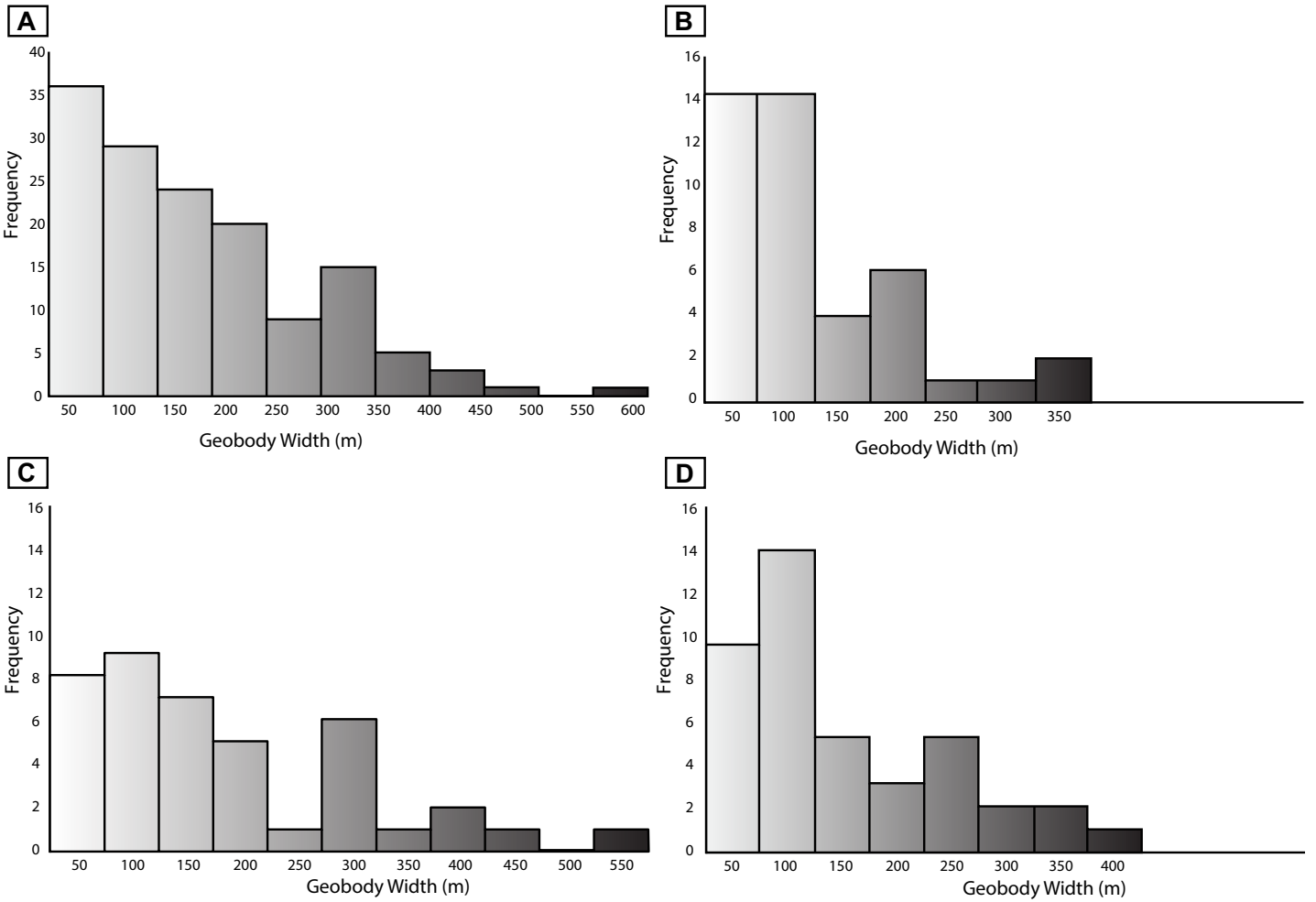

Figure 7. (A) Histogram plot of all corrected geobody widths in the La Serreta succession. (B) Histogram of the distribution of the maximum corrected geobody widths from the digitized geobodies identified in the digital outcrop models (DOMs). (C) Histogram of the distribution of the minimum corrected geobody widths. (D) Histogram of the distribution of calculated arithmetic mean of corrected geobody widths.

DISCUSSION

Sandstone Body Architecture

When examining the overall sandstone body widths in the medial portion of the Huesca fluvial fan, laterally continuous sandstone bodies constitute a significant proportion of the observed sandstone body architecture (Fig. 2). Sandstone bodies interpreted as multilateral/multistory deposits comprise the majority (78%) of the measured sandstone bodies, with single-story deposits as the subordinate type (22%; Table 2). Most of the sandstone deposits identified in this study are interpreted to be channel belts (μ = 127 m wide, μ max. = 372 m; Fig. 7). Some of the sandstone bodies do extend for hundreds of meters laterally (Fig. 7), with the multilateral/multistory sandstone bodies being the widest; however, most of all the measured

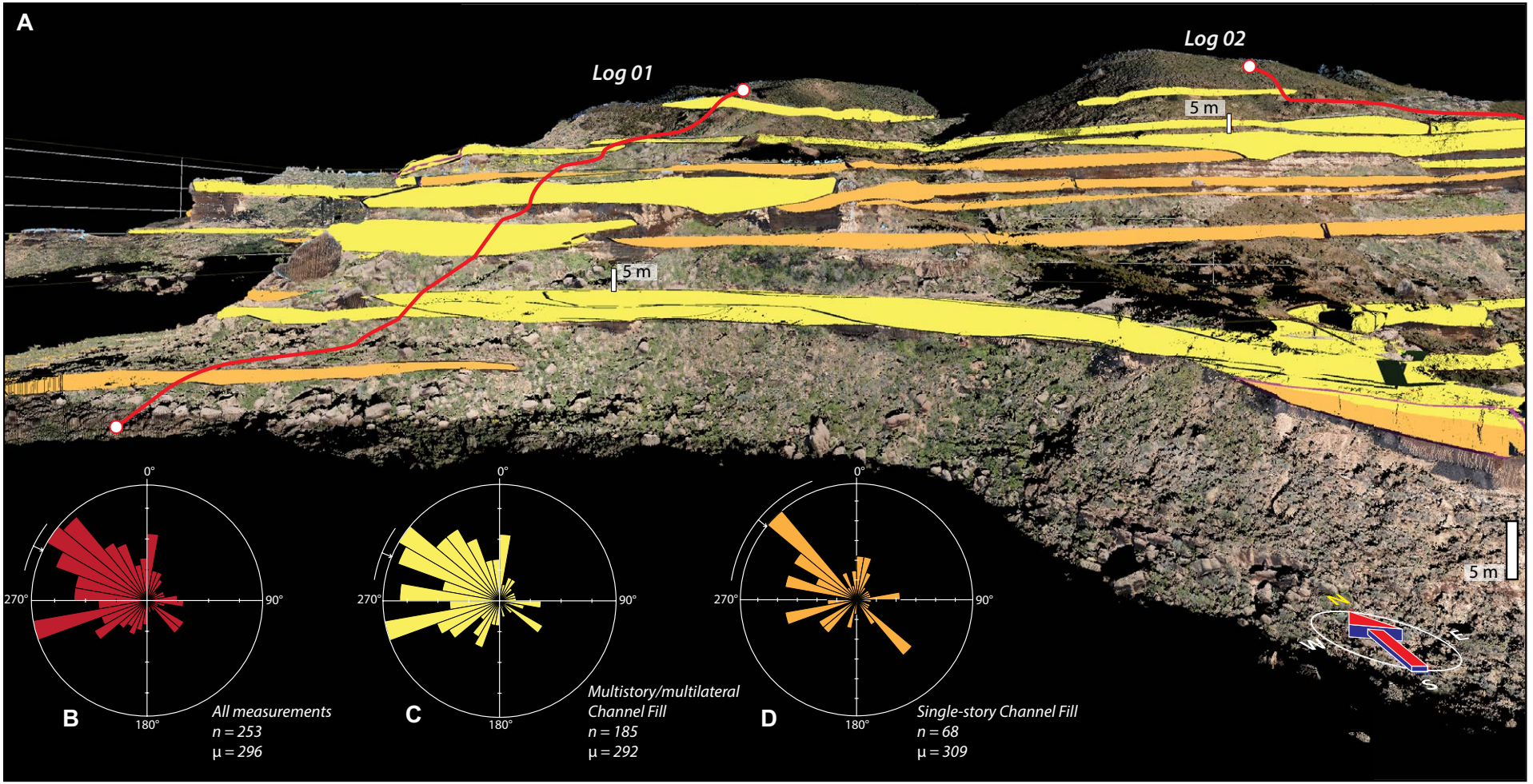

Figure 8. (A) Facies-classified sandstone bodies within the point cloud derived from the Geobody mapping tool in Virtual Reality Geological Studio (VRGS) software. Note the scale bar is 5 m. (B–D) Rose diagrams generated from paleocurrent information gathered from the field and sedimentary logs: (B) rose diagram generated from all measured paleocurrents that indicate an overall paleoflow of the section to the WNW direction (296°); (C) rose diagram attributed to interpreted multistory/multilateral channel elements, with a mean azimuth of 292° from 185 measurements; and (D) rose diagram derived from less common single-story channel elements, with a mean azimuth of 309° from 68 measurements.

geobodies (68.3%) are less than 150 m wide. These channels belts most likely produced the observed multilateral and multistory sandstone channel-fill elements, as the active channel would meander within the confines of the channel belt. This was also observed in previous work in La Serreta and other localities in the Huesca distributive fluvial system (Hirst, 1992; Fisher and Nichols, 2013). Other ancient distributive fluvial system deposits exhibit similar architecture within the medial zone of the respective system (e.g., Owen et al., 2017b). Additionally, sandstone body W:T relationships show a positive correlation (i.e., $R^2 = 0.5027$; Fig. 10) and suggest both ribbon and sheetlike geometries are present, when using ratio values defined by Friend et al. (1979). Half (50%) of interpreted sandstone bodies have ribbon-defined geometry (W:T < 15:1), with the other 50% classified as sheetlike geometries (W:T > 15:1), representing a 49% increase compared to the previously suggested value (e.g., Hirst, 1992).

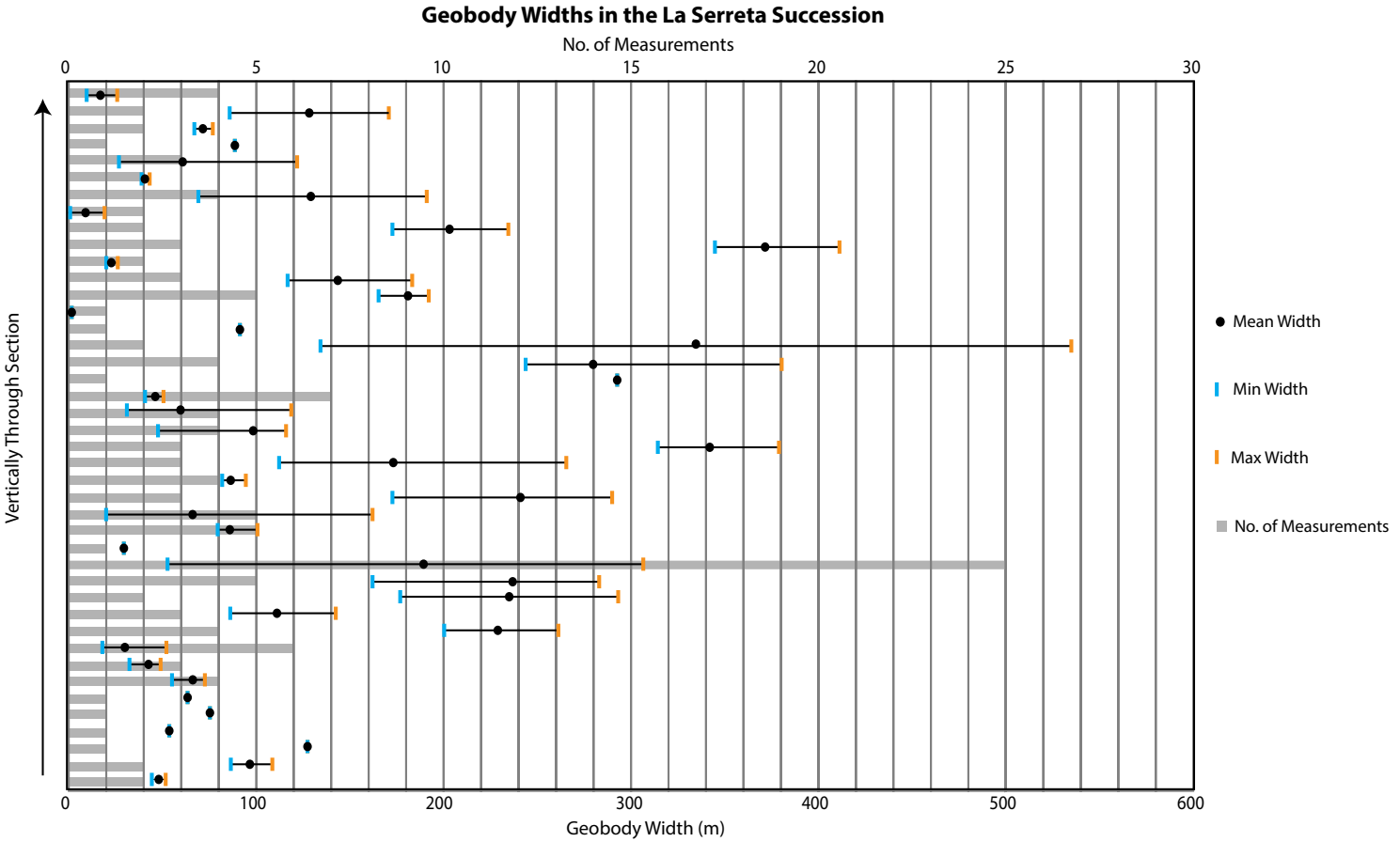

Figure 9. Plot of all 42 measured sandstone bodies in stratigraphic order, indicating temporal trends identified within the La Serreta section. Gray bars indicate the number of observations (paleo-flow measurements) used to calculate the probability distribution function (PDF) of corrected sandstone body widths for the associated measured sandstone body.

Previous analysis of the sandstone body geometries in the study area by Hirst (1992) were used by Gibling (2006) in his investigation of the relationship between width and thickness of different fluvial sandstone bodies. Sandstone bodies of the La Serreta section were placed into a similar plot in Figure 12, and polygons were drawn around the mean sandstone body width data points (purple polygon), and compared to those from Gibling (2006; light-blue). The minimum (blue) and maximum (orange) sandstone body measurements were used to develop a separate polygon (red dashed line with light-gray fill) to identify outliers (minimum and maximum data points) and uncertainty. These data indicate some sandstone bodies are thicker and less wide than identified in previous works (i.e., Hirst, 1992; Donselaar and Schmidt, 2005), and they indicate a general thickening and widening trend up section, with a decrease in width and thickness evident in the top quarter of the section (Fig. 9).

The observed sandstone body architecture is composed of a series of repeated sandstone body thickening and widening (Fig. 11), within an overall increase in sandstone body width and thickness up section. This observed increase in sandstone body width and thickness may be the product of several interrelated factors. Allogenic processes (i.e., tectonic uplift in the hinterland, climatic shift) are considered, as they would increase sediment supply to the active depositional lobe, or, conversely, a steady sediment supply with continued basin subsidence, allowing the active channel belt to remain in its spatial position before eventual avulsion took place (Sheets

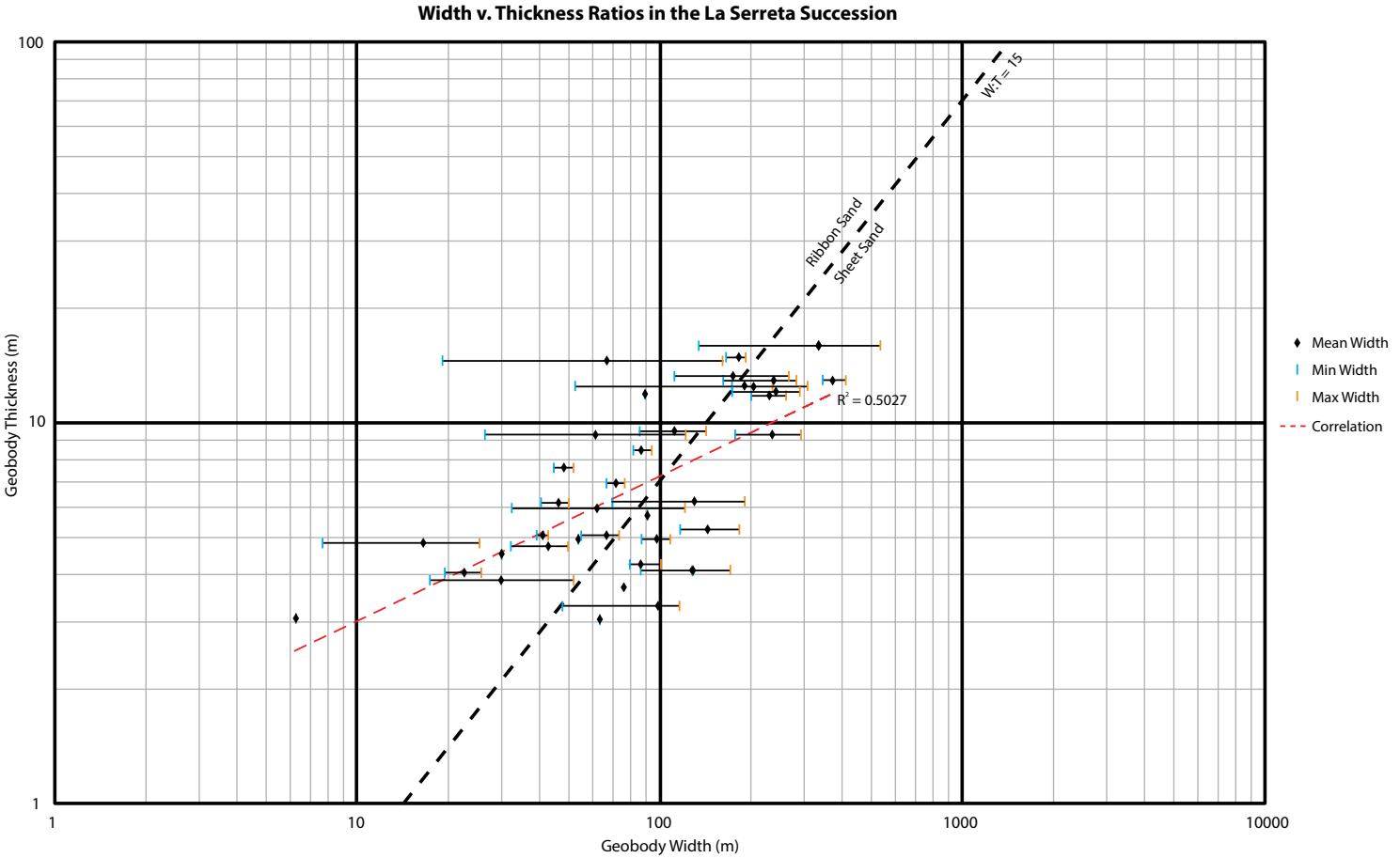

Figure 10. Width vs. thickness plot of the corrected geobody widths derived from the digital outcrop models (DOMs). The minimum, maximum, and arithmetic mean values are plotted for 42 different measured sandstone body geometries. The width to thickness ratio line (15:1), calculated according to Friend et al. (1979) to determine a difference between measured ribbon and sheet geometry, is digitized into the plot to visualize the distribution across the data. Line of best fit (red dashed) was plotted for the calculated mean geobody width, yielding an R^2 value of 0.5027.

et al., 2002). Autogenic processes are possible, such as increased avulsion in the area as the channel belts moved to occupy available accommodation within the depositional lobe. These avulsion events would have created recurring channel-fill and thick overbank elements as the active channel belt(s) continually avulsed across the alluvial plain in an effort to fill available accommodation. Aggradation of a fluvial system is suggested to be linked to avulsion frequency (Bryant et al., 1995) and, as observed in other distributive fluvial systems (e.g., Okavango Fan), aggradation rate increases down the fan (McCarthy et al., 1992). This suggests that during periods of aggradation, avulsion events are common in the medial to distal zones of a distributive fluvial system and are often coupled with lobe progradation (Weissmann et al., 2015). The progressive deposition and aggradation of the Huesca distributive fluvial system (Nichols, 2004) and the temporal trends present within the system (Figs. 9 and 12) suggest that an interplay between local avulsion process within the depositional lobe and basin-scale simultaneous progradation most likely produced the sandstone body architecture (Fig. 2) observed within the data (Fig. 9). This has been suggested in other works (i.e., Donselaar and Schmidt, 2010; Fisher and Nichols, 2013) through regional and local analyses of sections of the Huesca distributive fluvial system, and it is suggested from the data presented herein.

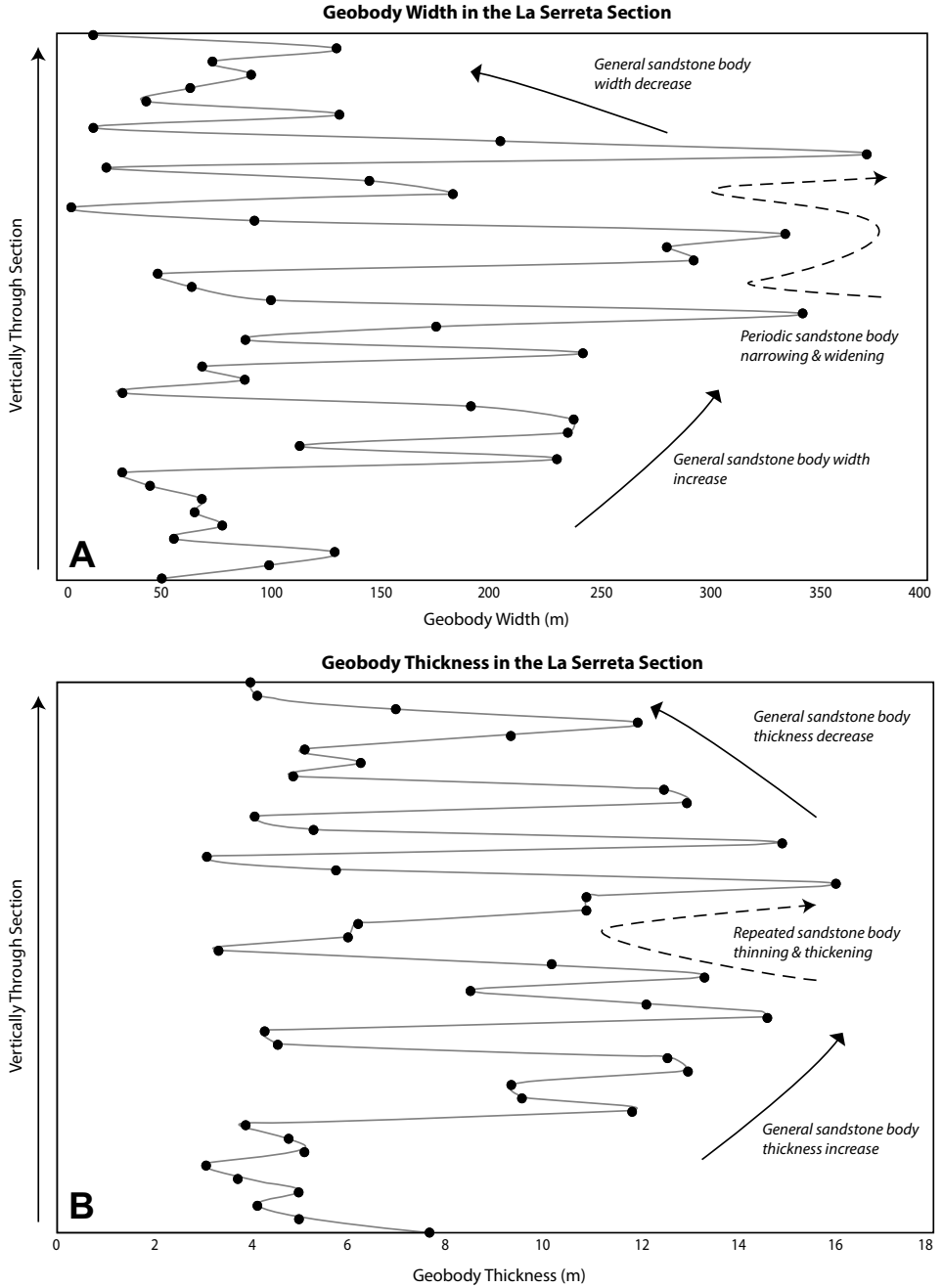

Figure 11. (A) Plot illustrating temporal trend in sandstone body widths up section. There is a periodic sandstone body widening and narrowing trend within an overall widening trend up section before a decrease in the top quarter of the section. (B) Plot illustrating a similar temporal trend in sandstone body thicknesses up section. These data indicate a periodic thickening and thinning with an overall up-section thickening trend before a general decrease in the top one third of the section.

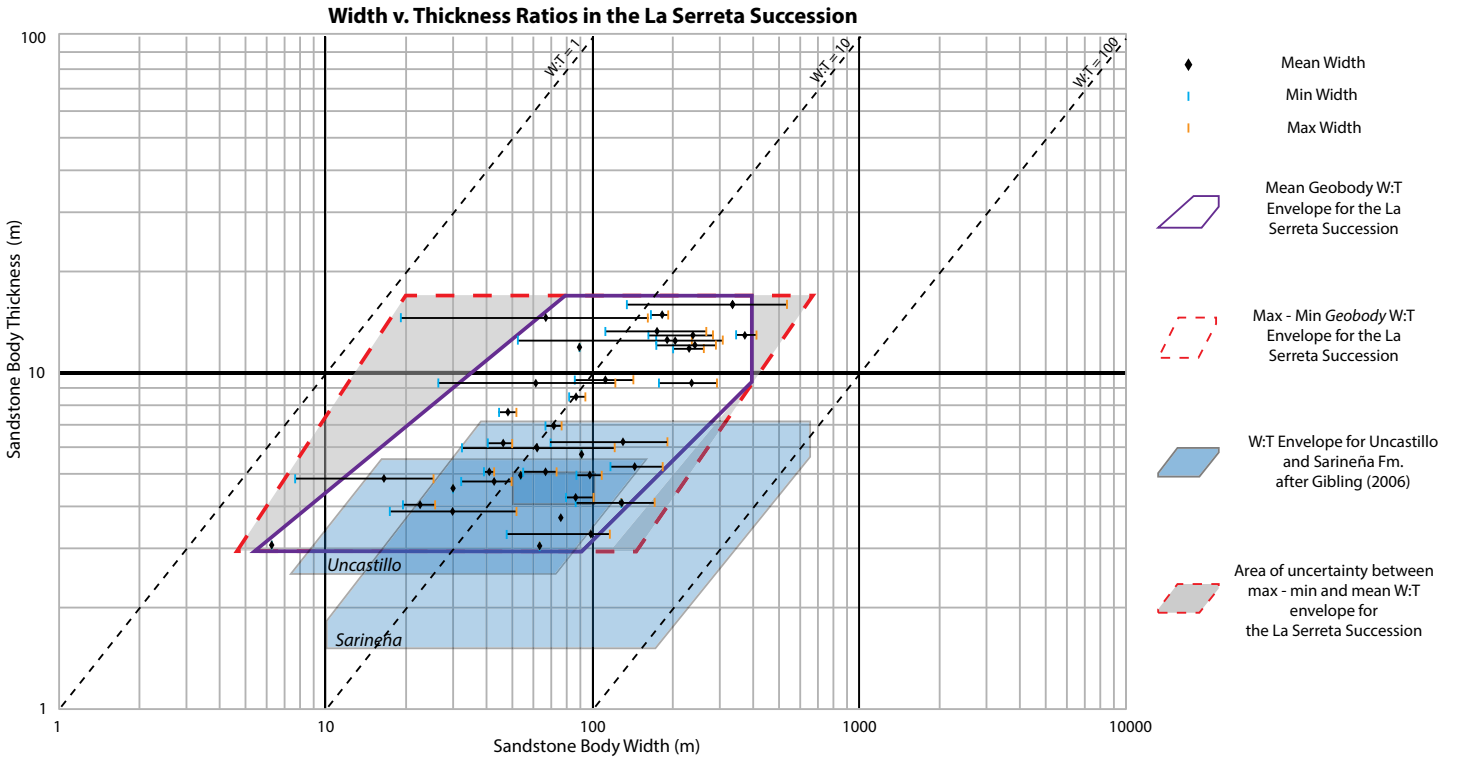

Figure 12. Plot of geobody width vs. thickness, with envelopes encompassing the arithmetic mean and minimum – maximum measurements from the corrected geobody widths. Red dashed envelopes indicate the minimum and maximum measurements for the geobody widths, while the gray fill highlights the associated uncertainties between the mean geobody width envelope and the min-max envelope. Note the translated location of the corrected geobody widths and thickness envelopes (purple and red dashed) from the quantified light detection and ranging (lidar) measurements compared to previous workers' data from the same formation (transparent blue; cf. Hirst [1992] and Gibling [2006]). W:T—sandstone body width to thickness ratio.

Finally, the decrease in sandstone body width and thickness evident at the top of the section suggests that active deposition ceased. It is likely that this was caused by avulsion of the distributive fluvial system away from the La Serreta area, or the cessation of deposition within the Huesca fluvial system, or subsequent erosion of deposits. Evidence of glacio-fluvial deposits is observed at the top of the section, which could explain the absence of recorded deposition by successive glacial erosion. The study area, however, is suggested to be a record of the last stage of fluvial fan development (Donselaar and Schmidt, 2010), most likely before the active channel belt, or lobe of the system, avulsed away from the La Serreta area for the final time. Therefore, the increase in sandstone body width and thickness is inferred to be a product of continued deposition of a channel within an active channel-belt present in the area at the time of deposition. The periodic sandstone body width and thickness increase, and decrease, up section is further evidence of successive avulsion events to and away from the La Serreta area until deposition ceased.

Implications for Reservoir Modeling

Bridge and Tye (2000) discussed the importance of accurately estimating the width and thickness of channel-fill deposits in the exploration and development of fluvial reservoirs. In the creation of accurate reservoir models, connectivity, both horizontal and vertical, is an essential element that can be used to understand and predict the reservoir potential of a system, especially for conventional fluvial reservoirs (Fielding and Crane, 1987; Miall, 1988). Connectivity and spatial distribution of sandstone bodies are commonly difficult to ascertain from 3-D seismic data because they often fall below resolvable resolution (Pranter et al., 2014). Even with high-resolution 1-D well data (e.g., borehole, wireline, or sedimentary logs), the lateral distance between them is often too great to resolve all lateral and vertical heterogeneity that exists, which can adversely affect connectivity and hydrocarbon sweep efficiency (Miall, 1988; Larue and Hovadik, 2006). Outcrop analogues can provide geoscientists with

TABLE 1. SANDSTONE BODY WIDTH AND THICKNESS PROBABILITY DISTRIBUTION FUNCTIONS (PDFs)

	N	Maximum (m)	Minimum (m)	Mean (m)	Std. dev.
Thickness	42	16.0	3.06	7.85	3.89
Sandstone body width PDFs					
Minimum width	42	344	6.18	98.4	84.2
Maximum width	42	535	25.1	158	125
Mean width	42	372	16.3	127	98.6

Note: Approximated sandstone body widths were calculated from digitized geobodies in Virtual Reality Geological Studio (VRGS) software, tabulated into minimum, maximum, and mean width measurements. These measurements are further tabulated into the minimum, maximum, mean, and standard deviation (Std. dev.) of those measurements.

data that fill in knowledge gaps that 1-D boreholes (i.e., spatial heterogeneity) and 3-D seismic (i.e., subseismic-scale elements) data cannot. The 2-D analyses of outcrop analogues is common procedure and employs the use of a combination of qualitative data (e.g., sedimentary logs, large photo panels, and architectural sketches). These practices, however detailed, can underestimate connectivity, because sandstone bodies may be partially exposed, and the orientation of the outcrop may not permit collection of essential sedimentological information (i.e., true width, channel sinuosity, continuity of sandstone bodies) required for accurate characterization of sandstone body geometry and architecture (Pringle et al., 2004; Fabuel-Perez et al., 2009a). These traditional approaches generally lack the necessary quantitative statistics and 3-D spatial control required for subsurface analogue construction.

To that end, it is of paramount importance that fluvial deposits and related outcrop analogues are evaluated in three dimensions to obtain quantitative conditioning and geostatistical data wherever possible. Reservoir connectivity and compartmentalization are inherently 3-D reservoir issues that must be addressed (Bryant et al., 2000; Pranter et al., 2014). The data presented herein however, show the type of 3-D geostatistical information extractable from DOMs, especially those of fluvial outcrop analogues (Fig. 9). The production of calculated sandstone body width PDFs for each measured sandstone body provides further constraining data that reservoir geoscientists can use in the modeling process. Additionally, the facies-classified point cloud data (Fig. 8) provide discreet input information that provides conditioning data for the facies modeling algorithms. Coupled together, these type of data-derived geostatistics provide essential information that geoscientists can use in the creation of accurate reservoir simulations.

Distributive fluvial systems are suggested to be a dominant depositional system in modern aggradational basins (Hartley et al., 2010; Weissmann et al., 2010), and recent work has highlighted the necessity for quantitative work in equivalent deposits in the rock record (e.g., Weissmann et al., 2013; Hartley et al., 2015; Owen et al., 2015, 2017a, 2017b). Similar fluvial deposits are present in a number of hydrocarbon reservoir systems (e.g., Ryseth et al., 1998; Nichols, 2005; Donselaar et al., 2011; Kukulski et al., 2013). These subsurface hydrocarbon reservoir systems rely on 1-D data that are spatially sparse and/or seismic data (2-D and 3-D) that commonly cannot resolve sandstone body geometries, which are essential to accurately model sandstone body connectivity (Darmadi et al., 2007; Pranter et al., 2014). As such, continued analysis of outcrop analogues for these systems is critical for accurate and effective reservoir modeling, especially digital outcrop studies, such as the one presented herein, which provide detailed geostatistical information that increases the sample size

TABLE 2. SANDSTONE BODY WIDTH AND ARCHITECTURE DISTRIBUTION

	N	Percentage component		
Distribution of sandstone body widths		0–150 m	150–300 m	>300 m
Minimum width	42	76.19%	19.05%	4.76%
Maximum width	42	59.52%	28.57%	11.90%
Mean width	42	69.05%	23.81%	7.14%
Distribution of sandstone body type				
Multilateral/multistory	42	78%		
Single story	42	22%		

Note: Distributions of all measured and corrected sandstone widths were categorized based on range of width values. Further distribution of sandstone bodies was classified by type (sensu Gibling, 2006).

of data used and reduces uncertainty in reservoir models (e.g., Fabuel-Perez et al., 2010; Labourdette, 2011; Pranter et al., 2014). The distribution of sandstone body types, corrected sandstone body widths, and the related PDFs presented herein provide reservoir geoscientists with a range of statistics that can be used in static object-based modeling procedures (Tables 1 and 2). Furthermore, there is and should continue to be a continuum of digital outcrop data collected for fluvial system analogues—from studies that cover large areas to provide regional statistics (e.g., Rittersbacher et al., 2013) to smaller-scale ones like the study presented herein for more detailed architectural analysis. These studies provide invaluable information that can be used to model channel-fill geometry across all scales within fluvial reservoir systems.

CONCLUSIONS

Digital outcrop studies such as the one presented herein increase the sample size of a geostatistical data set and illustrate the need for increased 3-D quantitative characterization and analysis of sandstone body widths and thickness relationships in fluvial sedimentary systems. We presented here an improved method that uses DOMs and their inherent quantitative attributes to map the spatial extents of sandstone bodies. The quantitatively mapped spatial extents of the exposed channel-fill elements produced a sample size of 42 different sandstone bodies. From the sandstone body analysis, preserved lithology in the La Serreta area records positive correlation between sandstone body width and thickness values, as well as a general up-section increase in sandstone body widths and thicknesses until the uppermost part of the exposed succession. A maximum sandstone body thickness of 16 m thick has been identified for the area, which is up to 6 m thicker than previously indicated. The narrowest sandstone bodies analyzed in this study indicate a minimum width of 6.18 m, representing a 3.82 m reduction compared to values identified by previous workers. Conversely, some of the sandstone bodies are up to 209 m wider than previously indicated. Furthermore, corrected sandstone body width and thickness relationships reveal that the La Serreta area contains 50% sheetlike and 50% ribbonlike sandstone bodies, a 49% increase from previous estimates. The increase in width and thickness observed are inferred to be a product of continued deposition of a channel within an active channel belt present in the area at the time of deposition. Periodic sandstone body width and thickness increase, and decrease, up section is further evidence of successive avulsion events to and away from the La Serreta area until deposition ceased.

Identification and acquisition of sandstone body information (i.e., width-to-thickness ratios, facies classifications, stratigraphic architecture) are integral to accurate predictions of heterogeneity, compartmentalization, and lateral and vertical connectivity within fluvial hydrocarbon reservoirs. The results presented herein further elucidate the necessity for 3-D quantitative analyses of outcrops used as analogues for hydrocarbon reservoirs and the geostatistics that can be obtained from them. Continued quantitative analyses of similar fluvial outcrop analogues remain paramount to gain further insight into architectural components that make up deposits within aggradational continental basins and particularly those used as analogues for the hydrocarbon industry.

ACKNOWLEDGMENTS

We gratefully acknowledge the financial support from Total S.A. for funding this work. We would like to thank W. Head, R. McAllister, and A. Newton for their assistance with the field data collection, and G. Heldreich for her valuable geological discussions in and out of the field. We would also like to thank Gary Nichols for his invaluable insight and discussions about the Huesca fluvial system and the Ebro Basin. We kindly thank Jerome Bellian, Peter Flaig, and Steve Hubbard for providing helpful suggestions and feedback that led to significant improvements to this manuscript.

REFERENCES CITED

Alexander, J., 1993, A discussion on the use of analogues for reservoir geology, *in* Ashton, M., ed., Advances in Reservoir Geology: Geological Society, London, Special Publication 69, p. 175–194, https://doi.org/10.1144/GSL.SP.1993.069.01.08.

Arenas, C., and Pardo, G., 1999, Latest Oligocene–late Miocene lacustrine systems of the north-central part of the Ebro Basin (Spain): Sedimentary facies model and palaeogeographic synthesis: Palaeogeography, Palaeoclimatology, Palaeoecology, v. 151, p. 127–148, https://doi.org/10.1016/S0031-0182(99)00025-5.

Arenas, C., Millan, H., Pardo, G., and Pocovi, A., 2001, Ebro Basin continental sedimentation associated with late compressional Pyrenean tectonics (north-eastern Iberia): Controls on basin margin fans and fluvial systems: Basin Research, v. 13, p. 65–89, https://doi.org/10.1046/j.1365-2117.2001.00141.x.

Bellian, J.A., Kerans, C., and Jennette, D.C., 2005, Digital outcrop models: Applications of terrestrial scanning LiDAR technology in stratigraphic modeling: Journal of Sedimentary Research, v. 75, p. 166–176, https://doi.org/10.2110/jsr.2005.013.

Bridge, J.S., and Tye, R.S., 2000, Interpreting the dimensions of ancient fluvial channel bars, channels, and channel belts from wireline-logs and cores: American Association of Petroleum Geologists Bulletin, v. 84, p. 1205–1228, https://doi.org/10.1306/A9673C84-1738-11D7-8645000102C1865D.

Bryant, I., Carr, D., Cirilli, P., Drinkwater, N., McCormick, D., Tilke, P., and Thurmond, J., 2000, Use of 3D digital analogues as templates in reservoir modelling: Petroleum Geoscience, v. 6, p. 195–201, https://doi.org/10.1144/petgeo.6.3.195.

Bryant, M., Falk, P., and Paola, C., 1995, Experimental study of avulsion frequency and rate of deposition: Geology, v. 23, p. 365–368, https://doi.org/10.1130/0091-7613(1995)023<0365:ESOAFA>2.3.CO;2.

Buckley, S.J., Howell, J.A., Enge, H.D., and Kurz, T.H., 2008, Terrestrial laser scanning in geology: Data acquisition, processing and accuracy considerations: Journal of the Geological Society [London], v. 165, p. 625–638, https://doi.org/10.1144/0016-76492007-100.

Burnham, B.S., and Hodgetts, D., 2015, Geologic modelling of geobody geometry and architecture of the Huesca distributive fluvial system, *in* 77th European Association of Geoscientists and Engineers (EAGE) Conference and Exhibition: Proceedings for the 2015 EAGE meeting, Madrid, Spain, p. 1–4, https://doi.org/10.3997/2214-4609.201412863.

Darmadi, Y., Willis, B.J., and Dorobek, S.L., 2007, Three-dimensional seismic architecture of fluvial sequences on the low-gradient Sunda Shelf, offshore Indonesia: Journal of Sedimentary Research, v. 77, p. 225–238, https://doi.org/10.2110/jsr.2007.024.

Donselaar, M.E., and Schmidt, J.M., 2005, Integration of outcrop and borehole image logs for high-resolution facies interpretation: Example from a fluvial fan in the Ebro Basin, Spain: Sedimentology, v. 52, p. 1021–1042, https://doi.org/10.1111/j.1365-3091.2005.00737.x.

Donselaar, M.E., and Schmidt, J.M., 2010, The application of borehole image logs to fluvial facies interpretation, *in* Poppelreiter, M., Garcia-Carballido, C., and Kraaijveld, M., eds., Dipmeter and Borehole Image Log Technology: American Association of Petroleum Geologists Memoir 92, p. 145–166, https://doi.org/10.1306/13181283M923415.

Donselaar, M.E., Overeem, I., Reichwein, J.H.C., and Visser, C.A., 2011, Mapping of fluvial fairways in the Ten Boer Member, southern Permian Basin, *in* Grötsch, J., and Gaupp, R., eds., The Permian Rotliegend of The Netherlands: Society for Sedimentary Geology (SEPM) Special Publication 98, p. 105–117, https://doi.org/10.2110/pec.11.98.0105.

Durkin, P.R., Hubbard, S.M., Boyd, R.L., and Leckie, D.A., 2015, Stratigraphic expression of intra-point-bar erosion and rotation: Journal of Sedimentary Research, v. 85, p. 1238–1257, https://doi.org/10.2110/jsr.2015.78.

Enge, H.D., Buckley, S.J., Rotevatn, A., and Howell, J.A., 2007, From outcrop to reservoir simulation model: Workflow and procedures: Geosphere, v. 3, p. 469–490, https://doi.org/10.1130/GES00099.1.

Fabuel-Perez, I., Hodgetts, D., and Redfern, J., 2009a, A new approach for outcrop characterization and geostatistical analysis of a low-sinuosity fluvial-dominated succession using digital outcrop models: Upper Triassic Oukaimeden Sandstone Formation, central High Atlas, Morocco: American Association of Petroleum Geologists Bulletin, v. 93, p. 795–827, https://doi.org/10.1306/02230908102.

Fabuel-Perez, I., Redfern, J., and Hodgetts, D., 2009b, Sedimentology of an intra-montane rift-controlled fluvial-dominated succession: The Upper Triassic Oukaimeden Sandstone Formation, central High Atlas, Morocco: Sedimentary Geology, v. 218, p. 103–140, https://doi.org/10.1016/j.sedgeo.2009.04.006.

Fabuel-Perez, I., Hodgetts, D., and Redfern, J., 2010, Integration of digital outcrop models (DOMs) and high resolution sedimentology—Workflow and implications for geological modelling: Oukaimeden Sandstone Formation, High Atlas (Morocco): Petroleum Geoscience, v. 16, p. 133–154, https://doi.org/10.1144/1354-079309-820.

Fernández, O., 2005, Obtaining a best fitting plane through 3D georeferenced data: Journal of Structural Geology, v. 27, p. 855–858, https://doi.org/10.1016/j.jsg.2004.12.004.

Fielding, C.R., and Crane, R.C., 1987, An application of statistical modelling to the prediction of hydrocarbon recovery factors in fluvial reservoir sequences, *in* Ethridge, F.G., Flores, R.M., and Harvey, M.D., eds., Recent Developments in Fluvial Sedimentology: Society of Economic Paleontologists and Mineralogists (SEPM) Special Publication 39, p. 321–327, https://doi.org/10.2110/pec.87.39.0321.

Fisher, J.A., and Nichols, G.J., 2013, Interpreting the stratigraphic architecture of fluvial systems in internally drained basins: Journal of the Geological Society [London], v. 170, p. 57–65, https://doi.org/10.1144/jgs2011-134.

Fisher, J.A., Nichols, G.J., and Waltham, D.A., 2007, Unconfined flow deposits in distal sectors of fluvial distributary systems: Examples from the Miocene Luna and Huesca systems, northern Spain: Sedimentary Geology, v. 195, p. 55–73, https://doi.org/10.1016/j.sedgeo.2006.07.005.

Friend, P.F., Slater, M.J., and Williams, R.C., 1979, Vertical and lateral building of river sandstone bodies, Ebro Basin, Spain: Journal of the Geological Society [London], v. 136, p. 39–46, https://doi.org/10.1144/gsjgs.136.1.0039.

Garcia-Castellanos, D., Vergés, J., Gaspar-Escribano, J., and Cloetingh, S., 2003, Interplay between tectonics, climate, and fluvial transport during the Cenozoic evolution of the Ebro Basin (NE Iberia): Journal of Geophysical Research–Solid Earth, v. 108, 2347, https://doi.org/10.1029/2002JB002073.

García-Sellés, D., Falivene, O., Arbués, P., Gratacos, O., Tavani, S., and Muñoz, J.A.A., 2011, Supervised identification and reconstruction of near-planar geological surfaces from terrestrial laser scanning: Computers & Geosciences, v. 37, p. 1584–1594, https://doi.org/10.1016/j.cageo.2011.03.007.

Gibling, M.R., 2006, Width and thickness of fluvial channel bodies and valley fills in the geological record: A literature compilation and classification: Journal of Sedimentary Research, v. 76, p. 731–770, https://doi.org/10.2110/jsr.2006.060.

Hartley, A.J., Weissmann, G.S., Nichols, G.J., and Warwick, G.L., 2010, Large distributive fluvial systems: Characteristics, distribution, and controls on development: Journal of Sedimentary Research, v. 80, p. 167–183, https://doi.org/10.2110/jsr.2010.016.

Hartley, A.J., Owen, A., Swan, A., Weissmann, G.S., Holzweber, B.I., Howell, J.A., Nichols, G.J., and Scuderi, L.A., 2015, Recognition and importance of amalgamated sandy meander belts in the continental rock record: Geology, v. 43, p. 679–682, https://doi.org/10.1130/G36743.1.

Hirst, J.P.P., 1992, Variations in alluvial architecture across the Oligo-Miocene Huesca fluvial system, Ebro Basin, Spain, *in* Miall, A.D., and Tyler, N., eds., The Three-Dimensional Facies Architecture of Terrigenous Clastic Sediments and its Implications for Hydrocarbon Discovery and Recovery: Society for Sedimentary Geology (SEPM) Concepts in Sedimentology and Paleontology 3, p. 111–121, https://doi.org/10.2110/csp.91.03.0111.

Hirst, J.P.P., and Nichols, G.J., 1986, Thrust tectonic controls on Miocene alluvial distribution patterns, southern Pyrenees, *in* Allen, P.A., and Homewood, P., eds., Foreland Basins: International Association of Sedimentologists Special Publication 8, p. 247–258, https://doi.org/10.1002/9781444303810.ch13.

Hodgetts, D., 2010, Collection, processing, interpretation and modelling of digital outcrop data using VRGS: An integrated approach to outcrop modelling, *in* 72nd European Association of Geoscientists and Engineers (EAGE) Conference and Exhibition—Workshops and Fieldtrips: Proceedings for the 2010 EAGE meeting in Barcelona, Spain, https://doi.org/10.3997/2214-4609.20149961.

Hodgetts, D., 2013, Laser scanning and digital outcrop geology in the petroleum industry: A review: Marine and Petroleum Geology, v. 46, p. 335–354, https://doi.org/10.1016/j.marpetgeo.2013.02.014.

Hodgetts, D., Seers, T., Head, W., and Burnham, B.S., 2015, High performance visualisation of multiscale geological outcrop data in single software environment, *in* 77th European Association of Geoscientists and Engineers (EAGE) Conference and Exhibition: Proceedings for the 2015 EAGE meeting in Madrid, Spain, https://doi.org/10.3997/2214-4609.201412862.

Jones, S.J., 2004, Tectonic controls on drainage evolution and development of terminal alluvial fans, southern Pyrenees, Spain: Terra Nova, v. 16, p. 121–127, https://doi.org/10.1111/j.1365-3121.2004.00539.x.

Kukulski, R.B., Hubbard, S.M., Moslow, T.F., and Raines, M.K., 2013, Basin-scale stratigraphic architecture of upstream fluvial deposits: Jurassic–Cretaceous foredeep, Alberta Basin, Canada: Journal of Sedimentary Research, v. 83, p. 704–722, https://doi.org/10.2110/jsr.2013.53.

Labourdette, R., 2011, Stratigraphy and static connectivity of braided fluvial deposits of the lower Escanilla Formation, south central Pyrenees, Spain: American Association of Petroleum Geologists Bulletin, v. 95, p. 585–617, https://doi.org/10.1306/08181009203.

Larue, D.K., and Hovadik, J., 2006, Connectivity of channelized reservoirs: A modelling approach: Petroleum Geoscience, v. 12, p. 291–308, https://doi.org/10.1144/1354-079306-699.

McCaffrey, K.J.W., Hodgetts, D., Howell, J., Hunt, D., Imber, J., Jones, R.R., Tomasso, M., Thurmond, J., and Viseur, S., 2010, Virtual fieldtrips for petroleum geoscientists, *in* Vining, B.A., ed., Petroleum Geology: From Mature Basins to New Frontiers—Proceedings of the 7th Petroleum Geology Conference: Geological Society, London, Petroleum Geology Conference Series Volume 7, p. 19–26, https://doi.org/10.1144/0070019.

McCarthy, T.S., Ellery, W.N., and Stainstreet, I., 1992, Avulsion mechanisms on the Okavango fan, Botswana: The control of a fluvial system by vegetation: Sedimentology, v. 39, p. 779–795, https://doi.org/10.1111/j.1365-3091.1992.tb02153.x.

Miall, A.D., 1988, Reservoir heterogeneities in fluvial sandstones: Lessons from outcrop studies: American Association of Petroleum Geologists Bulletin, v. 72, p. 682–697, https://doi.org/10.1306/703C8F01-1707-11D7-8645000102C1865D.

Nichols, G.J., 1987, Structural controls on fluvial distributary systems—The Luna system, northern Spain, *in* Recent Developments in Fluvial Sedimentology: Society of Economic Paleontologists and Mineralogists (SEPM) Special Publication 39, p. 269–277.

Nichols, G.J., 2004, Sedimentation and base level in an endorheic basin: The early Miocene of the Ebro Basin, Spain: Boletín Geológico y Minero, v. 115, p. 427–438.

Nichols, G.J., 2005, Sedimentary evolution of the Lower Clair Group, Devonian, West of Shetland: Climate and sediment supply controls on fluvial, aeolian and lacustrine deposition, *in* Doré, A.G., and Vining, B.A., eds., Petroleum Geology: North-West Europe and Global Perspectives—Proceedings of the 6th Petroleum Geology Conference: Geological Society, London, Petroleum Geology Conference Series Volume 6, p. 957–967, https://doi.org/10.1144/0060957.

Nichols, G.J., 2007, Fluvial systems in desiccating endorheic basins, *in* Nichols, G.J., Williams, E., and Paola, C., eds., Sedimentary Processes, Environments and Basins: A Tribute to Peter Friend: International Association of Sedimentologists Special Publication 38, p. 569–589, https://doi.org/10.1002/9781444304411.ch23.

Nichols, G.J., 2009, Fluvial systems in desiccating endorheic basins, *in* Nichols, G.J., Williams, E., and Paola, C., eds., Sedimentary Processes, Environments and Basins: A Tribute to Peter Friend: International Association of Sedimentologists Special Publication 38, p. 569–589, https://doi.org/10.1002/9781444304411.ch23.

Nichols, G.J., and Fisher, J.A., 2007, Processes, facies and architecture of fluvial distributary system deposits: Sedimentary Geology, v. 195, p. 75–90, https://doi.org/10.1016/j.sedgeo.2006.07.004.

Nichols, G.J., and Hirst, J.P.P., 1998, Alluvial fans and fluvial distributary systems—Oligo-Miocene, northern Spain: Contrasting processes and products: Journal of Sedimentary Research, v. 68, p. 879–889, https://doi.org/10.2110/jsr.68.879.

North, C.P., and Taylor, K.S., 1996, Ephemeral-fluvial deposits: Integrated outcrop and simulation studies reveal complexity: American Association of Petroleum Geologists Bulletin, v. 80, p. 811–830, https://doi.org/10.1306/64ED88D6-1724-11D7-8645000102C1865D.

Owen, A., Nichols, G.J., Hartley, A.J., Weissmann, G.S., and Scuderi, L.A., 2015, Quantification of a distributive fluvial system: The Salt Wash distributive fluvial system of the Morrison Formation, SW U.S.A.: Journal of Sedimentary Research, v. 85, p. 544–561, https://doi.org/10.2110/jsr.2015.35.

Owen, A., Ebinghaus, A., Hartley, A.J., Santos, M.G.M.M., and Weissmann, G.S., 2017a, Multi-scale classification of fluvial architecture: An example from the Paleocene–Eocene Bighorn Basin, Wyoming: Sedimentology, v. 64, p. 1572–1596, https://doi.org/10.1111/sed.12364.

Owen, A., Nichols, G.J., Hartley, A.J., and Weissmann, G.S., 2017b, Vertical trends within the prograding Salt Wash distributive fluvial system, SW United States: Basin Research, v. 29, p. 64–80, https://doi.org/10.1111/bre.12165.

Pranter, M.J., Hewlett, A.C., Cole, R.D., Wang, H., and Gilman, J., 2014, Fluvial architecture and connectivity of the Williams Fork Formation: Use of outcrop analogues for stratigraphic characterization and reservoir modelling, *in* Martinius, A.W., Howell, J.A., and Good, T.R., eds., Sediment-Body Geometry and Heterogeneity: Analogue Studies for Modelling the Subsurface: Geological Society, London, Special Publication 387, p. 57–83, https://doi.org/10.1144/SP387.1.

Pringle, J.K., Westerman, R., Clark, J.D., Drinkwater, N.J., and Gardiner, A.R., 2004, 3D high-resolution digital models of outcrop analogue study sites to constrain reservoir model uncertainty: An example from Alport Castles, Derbyshire, UK: Petroleum Geoscience, v. 10, p. 343–352, https://doi.org/10.1144/1354-079303-617.

Pringle, J.K., Howell, J.A., Hodgetts, D., Westerman, A.R., and Hodgson, D.M., 2006, Virtual outcrop models of petroleum reservoir analogues: A review of the current state-of-the-art: First Break, v. 24, p. 33–42, https://doi.org/10.3997/1365-2397.2006005.

Rarity, F., van Lanen, X.M.T., Hodgetts, D., Gawthorpe, R.L., Wilson, P., Fabuel-Perez, I., and Redfern, J., 2014, LiDAR-based digital outcrops for sedimentological analysis: Workflows and techniques, *in* Martinius, A.W., Howell, J.A., and Good, T.R., eds., Sediment-Body Geometry and Heterogeneity: Analogue Studies for Modelling the Subsurface: Geological Society, London, Special Publication 387, p. 153–183, https://doi.org/10.1144/SP387.5.

Rittersbacher, A., Buckley, S.J., Howell, J.A., Hampson, G.J., and Vallet, J., 2013, Helicopter-based laser scanning: A method for quantitative analysis of large-scale sedimentary architecture, *in* Martinius, A.W., Howell, J.A., and Good, T.R., eds., Sediment-Body Geometry and Heterogeneity: Analogue Studies for Modelling the Subsurface: Geological Society, London, Special Publication 387, p. 185–202, https://doi.org/10.1144/SP387.3.

Rittersbacher, A., Howell, J.A., and Buckley, S.J., 2014, Analysis of fluvial architecture in the Blackhawk Formation, Wasatch Plateau, Utah, U.S.A., using large 3D photorealistic models: Journal of Sedimentary Research, v. 84, p. 72–87, https://doi.org/10.2110/jsr.2014.12.

Ryseth, A., Fjellbirkeland, H., Osmundsen, I.K., Skålnes, Å., and Zachariassen, E., 1998, High-resolution stratigraphy and seismic attribute mapping of a fluvial reservoir: Middle Jurassic Ness Formation, Oseberg Field: American Association of Petroleum Geologists Bulletin, v. 82, p. 1627–1651, https://doi.org/10.1306/1D9BCB5B-172D-11D7-8645000102C1865D.

Sadler, S.P., and Kelly, S.B., 1993, Fluvial processes and cyclicity in terminal fan deposits: An example from the Late Devonian of southwest Ireland: Sedimentary Geology, v. 85, p. 375–386, https://doi.org/10.1016/0037-0738(93)90093-K.

Seers, T.D., and Hodgetts, D., 2014, Comparison of digital outcrop and conventional data collection approaches for the characterization of naturally fractured reservoir analogues, *in* Spence, G.H., Redfern, J., Aguilera, R., Bevan, T.G., Cosgrove, J.W., Couples, G.D., and Daniel, J.-M., eds., Advances in the Study of Fractured Reservoirs: Geological Society, London, Special Publication 374, p. 51–77, https://doi.org/10.1144/SP374.13.

Sheets, B.A., Hickson, T.A., and Paola, C., 2002, Assembling the stratigraphic record: Depositional patterns and time-scales in an experimental alluvial basin: Basin Research, v. 14, p. 287–301, https://doi.org/10.1046/j.1365-2117.2002.00185.x.

Teixell, A., 1996, The Ansó transect of the southern Pyrenees: Basement and cover thrust geometries: Journal of the Geological Society [London], v. 153, p. 301–310, https://doi.org/10.1144/gsjgs.153.2.0301.

van Lanen, X.M.T., Hodgetts, D., Redfern, J., and Fabuel-Perez, I., 2009, Applications of digital outcrop models: Two fluvial case studies from the Triassic Wolfville Fm., Canada, and Oukaimeden Sandstone Fm., Morocco: Geological Journal, v. 44, p. 742–760, https://doi.org/10.1002/gj.1196.

Weissmann, G.S., Hartley, A.J., Nichols, G.J., Scuderi, L.A., Olson, M., Buehler, H., and Banteah, R., 2010, Fluvial form in modern continental sedimentary basins: Distributive fluvial systems: Geology, v. 38, p. 39–42, https://doi.org/10.1130/G30242.1.

Weissmann, G.S., Hartley, A.J., Scuderi, L.A., Nichols, G.J., Davidson, S.K., Owen, A., Atchley, S.C., Bhattacharya, P., Chakraborty, T., Ghosh, P., Nordt, L.C., Michel, L., and Tabor, N.J., 2013, Prograding distributive fluvial systems—Geomorphic models and ancient examples, *in* Driese, S.G., Nordt, L.C., and McCarthy, P.J., eds., New Frontiers in Paleopedology and Terrestrial Paleoclimatology: Society for Sedimentary Geology (SEPM), Special Publication 104, p. 131–147, https://doi.org/10.2110/sepmsp.104.16.

Weissmann, G.S., Hartley, A.J., Scuderi, L.A., Nichols, G.J., Owen, A., Wright, S., Felicia, A.L., Holland, F., and Anaya, F.M.L., 2015, Fluvial geomorphic elements in modern sedimentary basins and their potential preservation in the rock record: A review: Geomorphology, v. 250, p. 187–219, https://doi.org/10.1016/j.geomorph.2015.09.005.

Xu, X., Aiken, C.L.V., Bhattacharya, J.P., Corbeanu, R.M., Nielsen, K.C., McMechan, G.A., and Abdelsalam, M.G., 2000, Creating virtual 3-D outcrop: The Leading Edge, v. 19, p. 197–202, https://doi.org/10.1190/1.1438576.